CHALMERS
UNIVERSITY OF TECHNOLOGY

MmWave Integrated Localization, Mapping, and Communication: A Stochastic Geometry Perspective

MmWave Integrated Localization, Mapping, and Communication: A Stochastic Geometry Perspective

Jiajun He†, Hien Quoc Ngo†, Han Yu†, Huiping Huang⋆, Henk Wymeersch⋆, and Michail Matthaiou†

†Centre for Wireless Innovation (CWI), Queen's University Belfast, BT3 9DT Belfast, U.K.
⋆Department of Electrical Engineering, Chalmers University of Technology, 41296 Göteborg, Sweden

***Abstract*—Sensing, as an underlying function of integrated sensing and communication (ISAC), can, in theory, enable numerous applications, including detection, localization, navigation, etc. However, in sixth generation (6G) and beyond, sensing data could be used in a more effective manner, while environmental mapping is a promising candidate to enhance the sensing capacity. This paper augments the conventional ISAC framework by introducing the concept of integrated localization, mapping, and communication (LMAC), exploring the feasibility of providing mapping services while maintaining localization accuracy. Closed-form expressions for the communication and localization signal-to-interference-plus-noise ratios (SINRs) are analytically derived to evaluate both the communication performance and the localizability of the localization user and scatterers. Furthermore, the Cramér-Rao lower bounds (CRLBs) for localization and mapping services are provided to characterize the fundamental limits of an LMAC system. Numerical results indicate that the proposed performance bounds effectively characterize the system performance and offer valuable insights into how different network configurations influence the performance and realizable potential of LMAC.**

***Index Terms*—Cramér-Rao lower bound, environmental mapping, integrated sensing and communication, millimeter-wave.**

I. Introduction

ISAC has garnered considerable attention as a representative technology in 6G, setting it apart from previous-generation networks. The primary functionalities of ISAC systems are to sense a target, e.g., a mobile device, and simultaneously provide reliable communication services to the communication user [1]. Meanwhile, the advancements in wireless communication technologies, such as millimeter wave (mmWave) networking, can underpin numerous applications, like digital twin, autonomous driving, surveillance, etc [2]. Nevertheless, in future and beyond-6G wireless networks, demanding requirements may emerge beyond those addressed by current ISAC systems [3], motivating us to seek alternative approaches.

Existing ISAC systems mainly rely on a single ISAC base station (BS) to sense the target while concurrently communicating with the mobile user, where the sensing data is primarily used for target localization [4]. To enhance the sensing capabilities of ISAC systems, the sensing data could be leveraged for higher-level services rather than merely detecting the presence and location of the target [5]. Building on the location-related information collected from the target, derivative applications, such as localization and tracking, are explored in the current literature [6]. In 6G and beyond wireless networks, sensing information should be harnessed in a more effective manner to enhance the communication performance and enable the possibility of higher-level services beyond those currently provided, while environmental mapping is a promising candidate for the next-generation ISAC [7].

In general, *mapping* involves transmitting sensing signals to environmental objects and analyzing the resulting echoes to extract location-related information for the registration of (static) landmarks in a map [8], while the constructed map can be leveraged to enhance both the sensing capability and communication performance of ISAC systems [9]. Nevertheless, incorporating the mapping into ISAC systems would entail additional challenges in multiple dimensions. For instance, inclusion of the mapping service complicates the beamforming design, as it requires balancing the performance of localization, mapping, and communication. The resource allocation strategy for LMAC systems is also more complex than in detection- or localization-only ISAC systems since allocating more power to mapping may undermine the performance of both communication and localization.

In this paper, we explore the feasibility of incorporating mapping services into the existing ISAC framework, namely LMAC. A unified analytical framework is developed to evaluate the fundamental limits of mmWave-based LMAC systems using stochastic geometry. We recall that the stochastic geometric framework has been widely adopted in analyzing the performance of ISAC systems [10]–[12], motivating its application to the LMAC system in this study. The contributions of this paper are listed as follows:

1) *SINR Distributions*: Considering the inherent randomness in the placements of transmitters (Txs), communication and localization users, and ambient objects, closed-form expressions for the communication and localization SINRs are analytically derived to characterize the communication performance, localizability of the user and scatterer points from ambient obstacles. The derived SINR expressions,

This work is supported by the U.K. Engineering and Physical Sciences Research Council (EPSRC) (grants No. EP/X04047X/1 and EP/X040569/1). The work of H. Q. Ngo and J. He was supported by the U.K. Research and Innovation Future Leaders Fellowships under Grant MR/X010635/1, and a research grant from the Department for the Economy Northern Ireland under the US-Ireland R&D Partnership Programme. The work of H. Huang was supported by the HORIZON-MSCA through the project NEAT-6G under Grant 101152670. The work of M. Matthaiou was supported by the European Research Council (ERC) under the European Union's Horizon 2020 research and innovation programme (grant agreement No. 101001331).

parameterized by various network configurations, serve as a guideline for the optimized design of LMAC systems.

2) *Localization Error Bound*: The localization error bound is derived to characterize the optimized achievable localization performance of the system. This error bound is parameterized by various network parameters, revealing how different network configurations influence the localization accuracy.
3) *Simple Mapping Bound*: A simplified and practical mapping error bound is derived to characterize the mapping capability of the proposed LMAC system, offering valuable insights for optimizing the network configurations to meet specific mapping requirements.

Remark 1. *Due to page limitations, the detailed derivations in the following analysis will be provided in the journal version.*

II. System Model

We consider a two-dimensional (2-D) LMAC configuration in which the LMAC-Txs, communication and localization users, and ambient objects are randomly distributed on a 2-D disk. Our objective is to enable communication with communication users, while simultaneously localizing localization users and conducting environmental perception. For the sake of tractability, we enumerate the following assumptions used throughout the performance analysis:

Assumption 1. *Each communication and localization user receives signals from its designated LMAC-Tx [10]–[13].*

Remark 2. *We assume that there are two types of mobile users: communication and localization users (receivers with unknown positions). During the localization and mapping process, the LMAC system localizes the localization user and estimates the position of scatterers resulting from passive objects.*

Assumption 2. *All ambient obstacles (reflectors) can reflect the transmitted signals, and independent blockage is assumed.*

Remark 3. *This assumption has been widely applied in wireless network modeling [14].*

Assumption 3. *The high-order reflection and scattering are neglected during the LMAC procedure.*

Remark 4. *Due to the severe propagation loss in mmWave transmission, only the line-of-sight (LoS) and first-order reflection paths are considered for user localization and environmental mapping, while the impact of the higher-order reflections can be neglected [8].*

Assumption 4. *Two-stage localization is adopted, where the location-related information has been extracted, while the measurement noise is assumed to be a zero-mean white Gaussian distributed.*

Remark 5. *This is a standard assumption in analyzing the performance of wireless localization systems [15].*

A. Network Model

The system model is depicted in Fig. 1, which represents a mmWave wireless network for 2-D LMAC. Without loss of generality, we assume that the typical localization user $\boldsymbol{\psi}_l = [x_l \ y_l]^T$ is located at the origin O, while the LMAC-Txs are randomly deployed in a 2-D disk with radius R_a by following the homogeneous Poisson point processes (HPPP) Φ_{Tx} with a density λ_{Tx}. The LMAC-Txs are equipped with a uniform linear array (ULA) deploying N_t antenna elements, while the localization users are equipped with a single omnidirectional antenna. The communication and localization users are randomly distributed within the 2-D disk, following a HPPP with a density of λ_u. It is noted that $\lambda_u \ll \lambda_{\text{Tx}}$. Furthermore, the Boolean line model (BLM) is utilized to randomly generate the ambient obstacles in the 2-D plane, where an ambient obstacle (reflector) is modeled as a line segment with length ℓ and inclination angle Θ, while ℓ and Θ are uniformly distributed in $[\ell_{\min}, \ell_{\max}]$ and $[0, \pi]$, respectively. The center point of the l-th line segment $\boldsymbol{x}_l$ also follows the HPPP Φ_r with density λ_r.

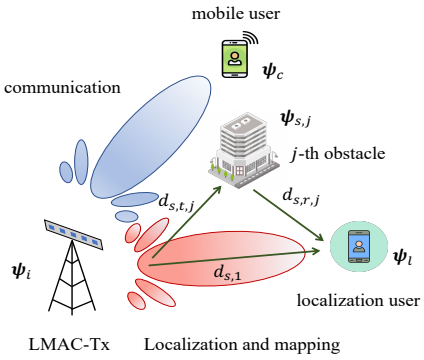

Fig. 1: Illustration of the considered LMAC system: The LMAC-Tx $\boldsymbol{\psi}_i$ transmits signals to the communication $\boldsymbol{\psi}_c$ and the localization $\boldsymbol{\psi}_l$ users, while the scatterer $\boldsymbol{\psi}_{s,j}$, generated by an obstacle, is estimated using the first-order reflection.

During the LMAC procedure, the i-th LMAC-Tx $\boldsymbol{\psi}_i$ transmits the signal $\boldsymbol{x}_i$ to both the nearest communication and localization users, which is written as: $\boldsymbol{x}_i = \sqrt{P_{t,i,c}}\boldsymbol{p}_c x_{c,i} + \sqrt{P_{t,i,s}}\boldsymbol{p}_s x_{s,i}$, where $\boldsymbol{p}_c$ and $\boldsymbol{p}_s$ are the beamformer and pilot for communication and localization, along with their associated transmitted symbols $x_{c,i}$ and $x_{s,i}$. The power allocated for communication and localization is $P_{t,i,c}$ and $P_{t,i,s}$, respectively. The received signal for the typical communication user is then:

$$y_{c,i} = \boldsymbol{h}_{c,i}^H \boldsymbol{x}_i + \sum_{\boldsymbol{\psi}_j \in \Phi_{\text{Tx}}, j \neq i} \boldsymbol{h}_{c,j}^H \boldsymbol{x}_j + n, \tag{1}$$

where $\boldsymbol{h}_{c,i}$ is the channel vector between the i-th LMAC-Tx and the typical communication user, n is the additive white Gaussian noise with power σ_n^2, and $(\cdot)^H$ is the conjugate transpose operation. Once the LMAC-Tx detects the localization user with sufficient SINR, it transmits N_s pilot symbols to the user for time-of-arrival (ToA) and angle-of-departure (AoD) estimation. Based on the received signals, the localization user then performs self-localization to determine its current location [10],[1] while the scatterer point resulting from the ambient

[1]This scenario is commonly observed in various commercial applications, such as targeted advertisement recommendations and user navigation in shopping malls and airports.

obstacle is estimated using the first-order reflection path, i.e., the environmental mapping. The total transmit power of the i-th LMAC-Tx is: $P_{t,i} = P_{t,i,s} + P_{t,i,c} \leq P_{\text{tot}}$.

B. Channel Model and Antenna Radiation Pattern

The signal attenuation in high-frequency systems, especially for mmWave transmissions, is mainly induced by the spreading loss, which is: $L_P(d) = (\frac{c}{4\pi f_s})^2 d^{-\alpha}$, where c is the speed of light, f_s and α are the signal operating frequency and path-loss exponent, respectively, while d is the signal propagation distance. During the LMAC process, both the localization and communication users may experience either LoS or non-line-of-sight (NLoS) conditions. Thus, the point process Φ_{Tx} can be divided into: $\Phi_{\text{Tx}}^{\text{L}}$ and $\Phi_{\text{Tx}}^{\text{N}}$, where the superscript L stands for the LoS and N for the NLoS [14, Assumption 4]. In addition, two types of blockages are considered, including:

1) *User Field of View*: The localization user is not able to connect with the detected LMAC-Tx within a cone with angle ω_s. Assuming that the user orientation is uniformly distributed in $[0, 2\pi]$, the probability that the localization user is not blocked by itself is given by: $p_s = 1 - \omega_s/2\pi$.
2) *Environmental Blockage*: The probability that the LoS link between the localization user and the nearest serving LMAC-Tx is not blocked is computed as: $p_b(d) = e^{-\beta d}$, where β is the blockage coefficient, which is determined by the density and geometry setting of the obstacles.

To conclude, the probability that the LMAC-Tx is not blocked is: $p_b^{\text{L}}(d) = (1-\omega_s/2\pi)e^{-\beta d}$ and $p_k^{\text{N}}(d) = 1-p_b^{\text{L}}(d)$. The multi-level flat-top (MLFT) antenna pattern is applied to approximate the actual antenna pattern for tractability, while the MLFT antenna gain function is [13]:[2]

$$G(\vartheta) = \begin{cases} G_i, & \text{if } \frac{2i-1}{N_t} - \frac{\bar{B}}{2} \leq |\vartheta| < \frac{2i-1}{N_t} + \frac{\bar{B}}{2}, \\ 0, & \text{otherwise}, \end{cases} \tag{2}$$

where ϑ is the cosine direction corresponding to the specific communication or localization user, $\bar{B}$ is the half-power beamwidth, where $1 \leq i \leq \lfloor N_t/2 \rfloor$, and $G_i = G_{\text{act}}(\frac{2i-1}{N_t})$, where $G_{\text{act}}(\vartheta) = \frac{\sin^2(\pi N_t \vartheta)}{N_t \sin^2(\pi \vartheta)}$ is the actual antenna pattern.

C. Communication SINR and User Localizability

Based on the received signal (1), the SINR measured by the typical communication user is given by:

$$\text{SINR}_{c,i} = \frac{\left|\sqrt{P_{t,i,c}}\boldsymbol{h}_{c,i}^H \boldsymbol{p}_c\right|^2}{\sigma_n^2 + I_{c,i}}, \tag{3}$$

$$I_{c,i} = \underbrace{\left|\sqrt{P_{t,i,s}}\boldsymbol{h}_{c,i}^H \boldsymbol{p}_s\right|^2}_{\text{Localization and mapping interference from serving LMAC-Tx}} + \underbrace{\sum_{\boldsymbol{\psi}_j \in \Phi_{\text{Tx}}, j \neq i} \left(\left|\sqrt{P_{t,j,c}}\boldsymbol{h}_{c,j}^H \boldsymbol{p}_c\right|^2 + \left|\sqrt{P_{t,j,s}}\boldsymbol{h}_{c,j}^H \boldsymbol{p}_s\right|^2 \right)}_{\text{Interference from remaining LMAC-Txs}}. \tag{4}$$

[2]Comparison of different antenna patterns was performed in [16], and the simulation results show that MLFT achieves the best approximation accuracy.

It was proved in [13], [14] that the numerator of (3) can be approximated by: $P_{t,i,c}G_{c,i}(\vartheta_{c,i})h_{c,i}(\frac{c}{4\pi f_s})^2 d_{c,i}^{-\alpha_{\text{L}}}$. Thus, the instantaneous communication SINR between the nearest serving LMAC-Tx and the typical communication user is:

$$\text{SINR}_{c,1} = \frac{P_{t,1,c}G_{c,1}(\vartheta_{c,1})h_{c,1}(\frac{c}{4\pi f_s})^2 d_{c,1}^{-\alpha_{\text{L}}}}{\sigma_n^2 + I_{c,1}}, \tag{5}$$

$$\begin{aligned} I_{\text{c},1} = \sum_{v \in \text{L,N}} \sum_{\boldsymbol{\psi}_i \in \Phi_s^v, i \neq 1} \Big(& P_{t,i,c}G_{c,i}(\vartheta_{c,i}) + \\ & P_{t,i,s}G_{s,i}(\vartheta_{s,i}) \Big) h_{s,i} d_{s,i}^{-\alpha_v} \\ & + G_{s,1}(\vartheta_{s,1}) P_{t,i,s} h_{c,1} d_{c,1}^{-\alpha_{\text{L}}}, \end{aligned} \tag{6}$$

where $d_{c,1}$ is the distance between the typical communication user and serving LMAC-Tx, α_v is the transmit power and path-loss exponent with $v = \{\text{L}, \text{N}\}$, while the beamforming gains $G_{c,j}(\vartheta_{c,j})$ and $G_{s,i}(\vartheta_{s,i})$ are computed based on (2). The effective channel gain $h_{c,i}$ follows a Gamma distribution Gamma$(M_v, 1/M_v)$ with Nakagami parameter M_v.[3] It is noted that the beamforming vector can be optimized based on user detection procedure, i.e.: $G_{c,1}(\vartheta_{c,1}) = N_t$. The localization SINR serves as an indicator of whether the LMAC-Tx can successfully detect the localization user, defined as target localizability in [17]. By following a similar manner as in (3) to (6), the instantaneous localization SINR between the nearest serving LMAC-Tx and the typical localization user is:

$$\text{SINR}_{s,1} = \frac{P_{t,1,s}G_{s,1}(\vartheta_{s,1})h_{s,1}(\frac{c}{4\pi f_s})^2 d_{s,1}^{-\alpha_{\text{L}}}}{\sigma_n^2 + I_{s,1}}, \tag{7}$$

where the interference $I_{s,1}$ can be computed as described in (6), while $d_{s,1} = \|\boldsymbol{\psi}_l - \boldsymbol{\psi}_1\|$ is the LoS distance between the localization user and serving LMAC-Tx. For the mapping SINR of the j-th scatter $\boldsymbol{\psi}_{s,j}$ (SINR$_{m,j}$), the LoS distance $d_{s,1}$ and the path-loss exponent α_{L} in the numerator of (7) are replaced with the reflecting distance $d_{\tau,t,j} = d_{s,t,j} + d_{s,r,j} = \|\boldsymbol{\psi}_i - \boldsymbol{\psi}_{s,j}\| + \|\boldsymbol{\psi}_{s,j} - \boldsymbol{\psi}_l\|$ and the NLoS path-loss exponent α_{N}, respectively.

D. Measurement Models

Since a two-step localization approach is assumed, the ToA and AoD from the direct path between the nearest serving LMAC-Tx and the typical localization user are given by [18]:[4]

$$\begin{aligned} r_{\tau,1} &= d_{s,1} + n_\tau, \\ r_{\phi,1} &= \phi_{s,1} + n_\phi = \tan^{-1}\left(\frac{y_i - y_l}{x_i - x_l}\right) + n_\phi, \end{aligned} \tag{8}$$

where n_τ and n_ϕ are the additive Gaussian noise terms of the ToA and AoD measurements with variance σ_τ^2 and σ_ϕ^2, respectively. It is noted that the range and angle variances are

[3]The Nakagami-m channel model is widely adopted for simulating channel gains in mmWave networks, particularly in scenarios with strong LoS components [13], [14].

[4]Based on Assumption 4, the ToA has been extracted for localization and mapping purposes. In practice, distance information can be acquired using round-trip time (RTT) or time-difference-of-arrival (TDoA)-based techniques.

computed by [18], [19]: $\sigma_\tau^2 = \frac{c^2}{f_s 8\pi^2 W E\{\text{SINR}_{s,1}\} N_s}$ and $\sigma_\phi^2 = \frac{6}{E\{\text{SINR}_{s,1}\}} \frac{1}{N_t(N_t-1)N_s}$, where W is the effective bandwidth and $E\{\cdot\}$ is the expectation operation; N_s is the number of transmit pilot symbols, while a larger number of N_s results in a lower measurement variance, thereby improving the accuracy of both the ToA and AoD estimates. For the mapping service, the scatterer point resulting from the environmental object is estimated using the reflecting distance between the LMAC-Tx and localization user through the j-th scatterer $\boldsymbol{\psi}_{s,j}$, while the corresponding ToA and AoD are given by [15]:

$$\begin{aligned} r_{\tau,t,j} &= d_{\tau,t,j} + n_\tau, \\ r_{\phi,t,j} &= \phi_{s,t,j} + n_\phi = \tan^{-1}\left(\frac{y_i - y_{s,j}}{x_i - x_{s,j}}\right) + n_\phi, \end{aligned} \tag{9}$$

where the range and angle variances can be computed as in (8), with the localization SINR replaced by the mapping SINR. By leveraging (8) and (9), the location estimates for the scatter and localization user can be obtained using maximum likelihood estimation [18], [20]. Identifying ambient obstacles using mapping information mitigates the blockage effect, thereby enhancing the average LoS range of the network. Thus, we assume that the reflector density λ_r is inversely proportional to the mapping accuracy (CRLB_m) [14], i.e.: $2\pi\lambda_r(1 - P(\text{CRLB}_m \leq s))$ and s is the stated accuracy, since the mapping assists the thinning operation of the BLM, thereby reducing λ_r.

III. SINR Distributions

The coverage probability of the typical communication user $\boldsymbol{\psi}_{c,1}$ is computed as [13], [14]:

$$\begin{aligned} &P(\text{SINR}_{c,1} > \tau_c) \\ &= P\left(\frac{P_{t,i,c} G_{c,1}(\vartheta_{c,1}) h_{c,1} (\frac{c}{4\pi f_s})^2 r_{c,1}^{-\alpha^{\text{L}}}}{\sigma_n^2 + I_{c,1}} \geq \tau_c\right), \end{aligned} \tag{10}$$

where τ_c is the communication threshold. The final expression of (10) is obtained by using the cumulative distribution function (CDF) of $h_{c,1}$, which is Nakagami-m distributed with parameters M_{L}, while the user localizability, i.e.: $P(\text{SINR}_{s,1} > \tau_s)$ and τ_s is the detection threshold, can be derived in a similar manner.

Proposition 1. *The distribution of the communication SINR is:*

$$\begin{aligned} P(\mathit{SINR}_{c,1} > \tau_c) &\simeq \sum_{m=1}^{M_{\text{L}}} \binom{M_{\text{L}}}{m} (-1)^{m+1} \\ &\times \int_0^{R_a} e^{-m e^{-M_{\text{L}}(M_{\text{L}}!)^{-\frac{1}{M_{\text{L}}}} \tau_c r_{c,1}^{\alpha_{\text{L}}} (\hat{\sigma}_n^2 + \hat{\sigma}_s^2)}} \\ &\times \mathcal{L}_{\hat{I}_{c,1}}\left(m e^{-M_{\text{L}}(M_{\text{L}}!)^{-\frac{1}{M_{\text{L}}}} \tau_c r_{c,1}^{\alpha_{\text{L}}}}\right) f_{r_{c,1}}(r) dr, \end{aligned} \tag{11}$$

$$\mathcal{L}_{\hat{I}_{c,1}}(s) = \prod_v \mathcal{L}_{\hat{I}_{c,1}^v}(s) = \prod_v \mathcal{L}_{\hat{I}_{c,1,c}^v}(s) \mathcal{L}_{\hat{I}_{c,1,s}^v}(s), \tag{12}$$

where $\hat{I}_{c,1,c}^v = \sum_{\boldsymbol{\psi}_i \in \Phi_{\text{Tx}}, i \neq 1} P_{t,i,c} G_{c,i}(\vartheta_{c,i}) h_{c,i} d_{c,i}^{-\alpha_v} / N_t$ *is the communication interference from the remaining LMAC-Tx, while the interference from localization and mapping resulting from the remaining LMAC-Tx is:* $\hat{I}_{c,1,s}^v = \sum_{\boldsymbol{\psi}_i \in \Phi_{\text{Tx}}, i \neq 1} P_{t,i,s} G_{s,i}(\vartheta_{c,i}) h_{c,i} d_{c,i}^{-\alpha_v} / N_t$, *while* $\hat{\sigma}_n^2 = \frac{\sigma_n^2}{P_{t,i,c} N_t} (\frac{4\pi f_s}{c})^2$. *The Laplace transform of* $\hat{I}_{c,1,c}^v$ *is:*

$$\begin{aligned} \mathcal{L}_{\hat{I}_{c,1,c}^v}(s) = \exp\Bigg(&4\pi\lambda_{\text{Tx}} \bar{B} \int_r^{R_a} p_b^v(r) \times \\ &\left(\sum_{n=1}^{\lfloor N_t/2 \rfloor} \left(1 + \frac{s G_{c,i}(\vartheta_{c,i}) h_{c,i} d_{c,i}^{-\alpha_v}}{N_t M_{\text{L}}}\right)^{M_{\text{L}}} - \left\lfloor \frac{N_t}{2} \right\rfloor\right) r dr\Bigg). \end{aligned} \tag{13}$$

Regarding the localization and mapping SINRs, we can derive their distributions by following (11) *to* (13)*.*

IV. Localization and Mapping Error Bounds

A. Localization Bound

The ToA and AoD measurements from the direct path are utilized for estimating the localization user ($\boldsymbol{\psi}_l$), while the CRLB is computed by: $\text{CRLB}_t = \text{tr}(\text{FIM}^{-1}(\boldsymbol{\psi}_l))$, where $\text{tr}(\cdot)$ is the trace operation, while the Fisher information matrix (FIM) is computed by: $\text{FIM}(\boldsymbol{\psi}_l) = \mathbb{E}\{-\frac{\partial^2 \ln p(r_{\tau,1}, r_{\phi,1}|\boldsymbol{\psi}_i)}{\partial \boldsymbol{\psi}_l \partial \boldsymbol{\psi}_l^H}\}$, while the joint probability density function (PDF) of the ToA and AoD measurements is:

$$\begin{aligned} p(r_{\tau,1}, r_{\phi,1}|\boldsymbol{\psi}_i) &= \frac{1}{\sqrt{2\pi\sigma_\tau^2}} \frac{1}{\sqrt{2\pi\sigma_\phi^2}} \times \\ &\exp\left(-\frac{1}{2\sigma_\tau^2}\left(r_{\tau,1} - \sqrt{(x_l - x_i)^2 + (y_l - y_i)^2}\right)^2\right) \\ &\exp\left(-\frac{1}{2\sigma_\phi^2}\left(r_{\phi,1} - \tan^{-1}\left(\frac{y_i - y_l}{x_i - x_l}\right)\right)^2\right). \end{aligned} \tag{14}$$

Proposition 2. *Given the range* (σ_τ^2) *and angular* (σ_ϕ^2) *errors, the CRLB for estimating the localization user is:*

$$\text{CRLB}_t = \text{tr}\left(\text{FIM}^{-1}(\boldsymbol{\psi}_l)\right) = \sigma_\tau^2 + d_{s,1}^2 \sigma_\phi^2, \tag{15}$$

where the FIM for the proposed localization problem is:

$$\begin{aligned} \text{FIM}(\boldsymbol{\psi}_l) &= \mathbb{E}\left\{-\frac{\partial^2 \ln p(r_{\tau,1}, r_{\phi,1}|\boldsymbol{\psi}_i)}{\partial \boldsymbol{\psi}_l \partial \boldsymbol{\psi}_l^H}\right\} \\ &= \begin{bmatrix} \frac{\cos^2\phi_{s,1}}{\sigma_\tau^2} + \frac{\sin^2\phi_{s,1}}{d_{s,1}^2\sigma_\phi^2} & \frac{\sin 2\phi_{s,1}}{2\sigma_\tau^2} - \frac{\sin 2\phi_{s,1}}{2d_{s,1}^2\sigma_\phi^2} \\ \frac{\sin 2\phi_{s,1}}{2\sigma_\tau^2} - \frac{\sin 2\phi_{s,1}}{2d_{s,1}^2\sigma_\phi^2} & \frac{\sin^2\phi_{s,1}}{\sigma_\tau^2} + \frac{\cos^2\phi_{s,1}}{d_{s,1}^2\sigma_\phi^2} \end{bmatrix}. \end{aligned} \tag{16}$$

B. Mapping Bound

Based on the reflection distance and AoD measurements in (9), the joint PDF is then given by:

$$\begin{aligned} p(r_{\tau,t,j}, r_{\phi,t,j}|\boldsymbol{\psi}_l, \boldsymbol{\psi}_i) &= \frac{1}{\sqrt{2\pi\sigma_\tau^2}} \frac{1}{\sqrt{2\pi\sigma_\phi^2}} \\ &\times \exp\left(-\frac{1}{2\sigma_\phi^2}\left(r_{\phi,t,j} - \tan^{-1}\left(\frac{y_i - y_{s,j}}{x_i - x_{s,j}}\right)\right)^2\right) \\ &\times \exp\left(-\frac{1}{2\sigma_\tau^2}\left(r_{\tau,t,j} - (d_{s,t,j} + d_{s,r,j})\right)^2\right). \end{aligned} \tag{17}$$

Note that in mmWave frequency bands, the values of σ_τ^2, σ_ϕ^2 are small, enabling high-precision localization and mapping.

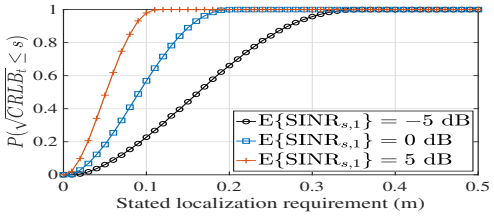

Fig. 2: Localization performance in terms of $P(\sqrt{\text{CRLB}_t} \leq s)$ for different values of $E\{\text{SINR}_{s,1}\}$ versus the localization accuracy.

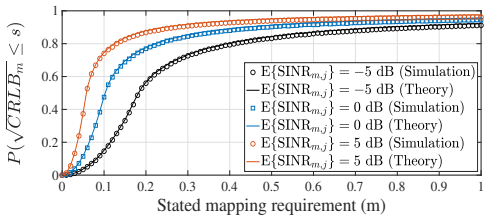

Fig. 3: Mapping performance in terms of $P(\sqrt{\text{CRLB}_m} \leq s)$ for different values of $E\{\text{SINR}_{m,j}\}$ versus the mapping accuracy (s).

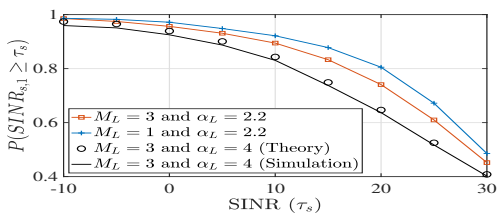

Fig. 4: Localizability $P(\text{SINR}_{s,1} \geq \tau_s)$ for different Nakagami shaping parameters M_{L} and path-loss exponents α_{L} versus τ_s.

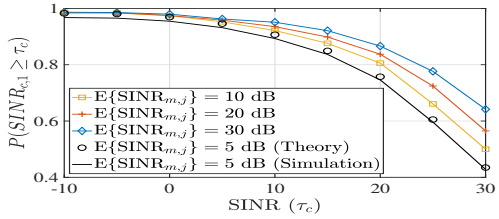

Fig. 5: Mapping-aided communication performance $P(\text{SINR}_{s,1} \geq \tau_s)$ for different values of $E\{\text{SINR}_{m,j}\}$ versus τ_c.

In addition, based on Proposition 2, the estimates of x_l and y_l are also Gaussian distributed with zero-mean and variance $\sigma_\tau^2 \cos^2\phi_{s,1} + d_{s,1}^2\sigma_\phi^2 \sin^2\phi_{s,1}$. The dependence of $\boldsymbol{\psi}_l$ can be averaged as described in [21, Eq. (4)]. The corresponding FIM is computed by:

$$\text{FIM}(\boldsymbol{\psi}_{s,j}) = \mathbb{E}\left\{-\frac{\partial^2 \ln p(r_{\tau,t,j}, r_{\phi,t,j}|\boldsymbol{\psi}_l, \boldsymbol{\psi}_i)}{\partial \boldsymbol{\psi}_{s,j} \partial \boldsymbol{\psi}_{s,j}^H}\right\}. \quad (18)$$

The CRLB for mapping the scatterer point is given by:

$$\text{CRLB}_m = \text{tr}(\text{FIM}^{-1}(\boldsymbol{\psi}_{s,j})) = \frac{A+B}{AB-C^2}, \quad (19)$$

$$\begin{aligned} A &= \frac{1}{\sigma_\tau^2}(\cos\phi_{s,t,j} + \cos\theta_{s,t,j})^2 + \frac{\sin^2\phi_{s,t,j}}{d_{s,t,j}^2\sigma_\phi^2}, \\ B &= \frac{1}{\sigma_\tau^2}(\sin\phi_{s,t,j} + \sin\theta_{s,t,j})^2 + \frac{\cos^2\phi_{s,t,j}}{d_{s,t,j}^2\sigma_\phi^2}, \\ C &= \frac{1}{\sigma_\tau^2}\left(\frac{\sin 2\phi_{s,t,j}}{2} + \sin(\phi_{s,t,j} + \theta_{s,t,j}) \right. \\ &\quad \left. + \frac{\sin 2\theta_{s,t,j}}{2}\right) - \frac{\sin 2\phi_{s,t,j}}{2d_{s,t,j}^2\sigma_\phi^2}, \end{aligned} \quad (20)$$

while $\theta_{s,t,j}$ is the associated angle-of-arrival and $[\boldsymbol{A}]_{i,j}$ represents the (i,j)-th entry of the matrix $\boldsymbol{A}$. However, the mapping CRLB in (19) is complex and lengthy, making it challenging to be optimized and derive its distribution, motivating us to approximate it using the following proposition.

Proposition 3. *Given the range and angle errors and the location of the localization user, the CRLB for mapping the scatter point can be approximated by:*

$$\text{CRLB}_m \approx \sigma_\phi^2 \frac{(4d_{s,t,j}^2 + \lambda)}{2(1+\cos\phi_{s,t,j})} \text{ and } \lambda = \sigma_\tau^2/\sigma_\phi^2. \quad (21)$$

Propositions 2 and 3 characterize the localization and mapping errors through simple CRLB expressions. By tuning the network parameters, system designers can gain insights into achieving the desired performance without the need for extensive simulations.

V. Simulation Results

A. Simulation Setup

The system performance in a mmWave (f_s = 30 GHz, W = 100 MHz) network is evaluated using 10^5 realizations. The LMAC procedure is simulated in a circular area with radius R_a = 50 m and a center point O. The typical localization user is located at O, while the mmWave LMAC-Txs and mobile users, and ambient obstacles are randomly deployed with densities $\lambda_{\text{Tx}} = 5\times10^{-3}/m^2$, $\lambda_u = 10^{-3}$, and $\lambda_r = 10^{-3}$. The transmit power of each LMAC-Tx is P_t = 30 dBm, the number of transmit pilot symbols for localization and mapping is: $N_s = 5$, while the thermal noise power is $\sigma_n^2 = -85$ dBm. The path-loss exponents and Nakagami-m parameters for the LoS and NLoS clusters are $\alpha_{\text{L}} = 2.2$, $\alpha_{\text{N}} = 4$, and $M^{\text{L}} = 3$, $M^{\text{N}} = 1$, respectively. In addition, $\beta = 0.01$, controls the severity of the blockage effect, while we set the user field of view to an angle of 60°. The length and inclination angle of the reflector are uniformly distributed in $[5, 15]$ m and $[0, \pi]$ rad. The antenna gain of each node is simulated using the MLFT antenna pattern, and we set $N_t = 16$.

B. Localization and Mapping Performance

The localization and mapping performance of the LMAC system is illustrated in Figs. 2 and 3, where the network geometries are randomly generated as described in Section V-A. It is seen in Fig. 2 that a higher $E\{\text{SINR}_{s,1}\}$ is observed to enhance the localization performance $P(\sqrt{\text{CRLB}_t} \leq s)$ of the LMAC system, underscoring the importance of optimizing the network configurations to improve the localization SINR. The accuracy of the approximated mapping bound (21) is shown in Fig. 3. It is seen that the mapping performance $P(\sqrt{\text{CRLB}_m} \leq s)$ produced by (21) closely aligns with the exact CRLB given in (19) across various SNR values, validating the accuracy of the proposed approximation strategy. Compared

to the lengthy and complex expression of the exact CRLB, the localization and mapping errors can be effectively characterized using the simplified expression provided in Propositions 2 and 3. Since the error bounds are formulated as a function of the measurement errors, the system designers can avail of these insights to optimize the system configuration and achieve the desired mapping accuracy. Furthermore, the localization CRLB exhibits higher accuracy compared to the mapping CRLB. This is attributed to the fact that the ToA and AoD measurements from the LoS path are utilized for user position estimation, which inherently experience lower measurement errors compared to those obtained from first-order reflections. Thus, enhancing the mapping SINR is crucial for achieving acceptable mapping performance.

C. Localizability and Mapping-assisted Communication

Figure 4 illustrates the localizability of the localization user in terms of the localization SINR given by (7). It is observed that the theoretical calculation (circle) generated by Proposition 1 is very close to the simulation results (solid line), justifying the correctness of our analysis. Increasing the Nakagami-m shaping parameter, M_{L}, enhances the localization SINR, which is intuitive since a higher M_{L} corresponds to a stronger LoS component. In addition, Fig. 4 shows the impact of the path-loss exponent on the localization SINR of the LMAC system. It is seen that the localization SINR decreases as the path-loss exponent increases. The path-loss exponent governs the severity of environmental blockage effects, resulting in a significant deterioration of the localization SINR performance. Therefore, optimizing the network configurations is crucial to ensuring an adequate SINR level for reliable localization and mapping performance. Compared with traditional ISAC systems, which physically separate the sensing and communication functionalities, the proposed LMAC system aims to leverage the mapping information to assist the communication process, while a higher performance of the mapping service reduces the blockage effect. Figure 5 illustrates that the communication performance improves with an increase in the mapping SINR. As a higher value of $E\{\mathrm{SINR}_{m,j}\}$ enhances the mapping performance, a better accuracy in the mapping service results in a lower density of the obstacles. This highlights the advantages of integrating the mapping service into the ISAC system. Nevertheless, improving the communication performance can lead to degradation in localization and mapping SINRs. Therefore, achieving an appropriate balance among communication, localization, and mapping is essential for practical LMAC implementation.

VI. Conclusion

This paper introduced the LMAC paradigm, which could enhance the sensing capabilities of ISAC systems by incorporating a mapping service. Tractable expressions for the communication and localization SINRs were derived to illuminate how various network parameters influence the communication performance and localizability of both the localization user and ambient obstacles. Furthermore, simple CRLBs were provided to characterize the localization and mapping errors of the LMAC system. Simulation results demonstrated that the LMAC system not only underpins the communication and sensing performance but also can utilize the mapping information to enhance the communication quality, thereby establishing a new paradigm for next-generation ISAC.

References

[1] F. Liu *et al.*, "Integrated sensing and communications: Toward dual-functional wireless networks for 6G and beyond," *IEEE J. Sel. Areas Commun.*, vol. 40, no. 6, pp. 1728–1767, Mar. 2022.

[2] A. Liu *et al.*, "A survey on fundamental limits of integrated sensing and communication," *IEEE Commun. Surveys Tuts.*, vol. 24, no. 2, pp. 994–1034, Feb. 2022.

[3] H. Wymeersch *et al.*, "6G positioning and sensing through the lens of sustainability, inclusiveness, and trustworthiness," *IEEE Wireless Commun.*, vol. 32, no. 1, pp. 68–75, Feb. 2025.

[4] F. Liu *et al.*, "Cramér-Rao bound optimization for joint radar-communication beamforming," *IEEE Trans. Signal Process.*, vol. 70, pp. 240–253, Dec. 2022.

[5] F. Dong *et al.*, "Sensing as a service in 6G perceptive networks: A unified framework for ISAC resource allocation," *IEEE Trans. Wireless Commun.*, vol. 22, no. 5, pp. 3522–3536, May 2023.

[6] Z. Wei *et al.*, "Integrated sensing, navigation, and communication for secure UAV networks with a mobile eavesdropper," *IEEE Trans. Wireless Commun.*, vol. 23, no. 7, pp. 7060–7078, Jul. 2024.

[7] J. Yang *et al.*, "Multi-domain cooperative SLAM: The enabler for integrated sensing and communications," *IEEE Wireless Commun.*, vol. 30, no. 1, pp. 40–49, Mar. 2023.

[8] A. Fascista *et al.*, "Downlink single-snapshot localization and mapping with a single-antenna receiver," *IEEE Trans. Wireless Commun.*, vol. 20, no. 7, pp. 4672–4684, Mar. 2021.

[9] H. Que *et al.*, "Joint beam management and SLAM for mmWave communication systems," *IEEE Trans. on Commun.*, vol. 71, no. 10, pp. 6162–6179, Jul. 2023.

[10] X. Gan *et al.*, "Coverage and rate analysis for integrated sensing and communication networks," *IEEE J. Sel. Areas Commun.*, vol. 42, no. 9, pp. 2213–2227, Jun. 2024.

[11] N. R. Olson, J. G. Andrews, and R. W. Heath Jr., "Coverage and rate of joint communication and parameter estimation in wireless networks," *IEEE Trans. Inf. Theory*, vol. 70, no. 1, pp. 206–243, Nov. 2024.

[12] K. Meng *et al.*, "Network-level integrated sensing and communication: Interference management and BS coordination using stochastic geometry," *IEEE Trans. Wireless Commun.*, vol. 23, no. 12, pp. 19365–19381, Dec. 2024.

[13] X. Yu *et al.*, "Coverage analysis for millimeter wave networks: The impact of directional antenna arrays," *IEEE J. Sel. Areas Commun.*, vol. 35, no. 7, pp. 1498–1512, Apr. 2017.

[14] T. Bai and R. W. Heath Jr., "Coverage and rate analysis for millimeter-wave cellular networks," *IEEE Trans. Wireless Commun.*, vol. 14, no. 2, pp. 1100–1114, Oct. 2015.

[15] Y. Zhang and K. C. Ho, "Localization of transmitters and scatterers by single receiver," *IEEE Trans. Signal Process.*, vol. 71, pp. 2267–2282, Jun. 2023.

[16] N. Deng and M. Haenggi, "A novel approximate antenna pattern for directional antenna arrays," *IEEE Commun. Lett.*, vol. 7, no. 5, pp. 832–835, Apr. 2018.

[17] C. E. O'Lone, H. S. Dhillon, and R. M. Buehrer, "Single-anchor localizability in 5G millimeter wave networks," *IEEE Wireless Commun. Lett.*, vol. 9, no. 1, pp. 65–69, Jan. 2020.

[18] H. C. So, *Source Localization: Algorithms and Analysis*. Ch. 3, pp. 59-106, John Wiley & Sons, Ltd, 2019.

[19] P. Stoica and A. Nehorai, "MUSIC, maximum likelihood, and Cramer-Rao bound," *IEEE Trans. Acoust., Speech, Signal. Process.*, vol. 37, no. 5, pp. 720–741, May 1989.

[20] W. Xiong *et al.*, "An ADMM approach for elliptic positioning in non-line-of-sight environments," *Digital Signal Processing*, vol. 154, p. 104653, Jun. 2024.

[21] J. He *et al.*, "Cramér-Rao lower bound analysis for elliptic localization with random sensor positions," *IEEE Trans. Aerosp. Electron. Syst.*, vol. 60, no. 4, pp. 5587–5595, Aug. 2024.